Journal of Structural Geology, Vol. 14, No. 4, pp. 405 to 424, 1992
Printed in Great Britain

0191-8141/92 $05.00+0.00
© 1992 Pergamon Press plc

Laboratory modelling of strain variation across rheological boundaries

SUSAN H. TREAGUS

Department of Geology, University of Manchester, Manchester M13 9PL, U.K.

and

DIMITRIOS SOKOUTIS

The Hans Ramberg Tectonic Laboratory, Department of Mineralogy and Petrology, Institute of Geology, Uppsala University, S-75122 Uppsala, Sweden

(*Received* 5 *March* 1991; *accepted in revised form* 17 *October* 1991)

Abstract—Laboratory models using viscous and viscoplastic silicones to simulate strain variation across competence contrasts are presented. This provides a test for earlier theoretical modelling of strain refraction in layers with Newtonian viscosity contrast, and a method of examining refraction rules for non-Newtonian materials. The main purpose is to test the theoretical rule that the finite shear strain ratio across a boundary is equivalent to the inverse viscosity ratio. Results for simple-shear experiments confirm this within the errors of viscometry and strain measurement. We investigate whether this rule applies to non-Newtonian materials, which necessarily involves a discussion on the nature of viscosity contrast for non-linear materials such as power-law fluids, and its bearing on competence contrasts in rocks.

These models also provide data on strain gradients generated by viscosity boundaries, which was not included in the earlier theoretical analyses. In the simple-shear experiments, the normalized shear strain profiles indicate an approximately linear shear stress gradient from the viscosity boundaries. Using an idealized linear shear strain gradient in a Newtonian matrix approaching a contrasting layer, we can derive expressions to predict the viscosity ratio. This may be a viable method of determining approximate viscosity ratios for more general deformations.

INTRODUCTION

Competence and the rheology of rock

THE variation in behaviour of rocks in deformation is commonly known as *competence* or *competence contrast*. Ramsay & Huber (1987, p. 12) describe competence as "the ease with which a material can deform", and use a dual definition of relative competence in terms of both ductile and brittle strength. Means (1990) restricts the definition to the brittle strength of materials. However, we find that 'competence' is most widely used as a measure of (inverse) relative ductility, as considered in detail by Ramsay (1982). We shall continue with this use of competence as a measure of the resistance to pervasive (ductile in the loose sense) deformation. The most important question, then, is the meaning of competence in the *material* sense. The answer must depend on the nature and meaning of viscosity for deforming rocks: the rheology of flowing rocks. We cannot hope to review all the relevant work in this field, so refer readers to recent reviews by Schmid (1982), Carter & Tsenn (1987), Kirby & Kronenberg (1987), Paterson (1987), Tsenn & Carter (1987) and Handy (1990) which provide a wealth of data and theory on the flow of rocks in the laboratory and in nature.

The creep or flow of materials may be considered, in theory, to fall into three broad groups (Tsenn & Carter 1987) at progressively increasing deformation rate: (i) diffusional creep which is equivalent to Newtonian fluid flow; (ii) power-law or dislocation creep which behaves according to a 'power-law' or Reiner–Rivlin fluid; and (iii) exponential creep. Laboratory creep tests on rocks have not conclusively confirmed diffusional creep. However, there has been a long tradition of theoretical modelling of ductile structures by Newtonian flow laws, which considerably predates laboratory creep experiments.

The above cited reviews of rock rheology reveal that a wide variety of rocks are found to flow by power-law creep according to the (simplified) Weertman relation (for two-dimensional flow) $\dot{\varepsilon} = A\sigma^n$, where $\dot{\varepsilon}$ is a steady-state strain rate, σ is the differential stress, A is a material constant and n is the 'stress exponent'. Summaries of values of A and n for different rock types are provided by Carter & Tsenn (1987, table 4) and Kirby & Kronenberg (1987, table 3). n values are from 1 to >10, with many values in the 3–6 range. However, Schmid (1982) has shown that for the same rock type, n may vary greatly according to the deformation mechanism. Paterson (1987) concluded that extrapolation from experiments to nature must be made with caution. To date, only a few rock types have been examined extensively, and flow in polymineralic rocks is not yet well understood (see Handy 1990).

There is an additional problem with applying the results of laboratory creep experiments to the flow of rocks under natural deformation conditions, highlighted by Hobbs (1972, p. 247): "For deformation by steady shortening all simple fluids behave as Reiner–Rivlin fluids [Truesdell & Noll 1965, pp. 472–473]. . . . Thus the power laws quoted for geological and metallurgical

materials and obtained from steady-state creep experiments are to some extent the result of the experimental technique and not of the material being deformed". This quotation would seem to be important and relevant to any review of rock rheology, and the question of whether rocks flow according to the 'power law'. It may also be relevant to the considerable number of analogue materials which laboratory measurements show to be approximately 'power law' (e.g. Plasticine, McClay 1976; silicone putties, Weijermars 1986a; paraffin wax, Mancktelow 1988), including the materials described later in this paper.

We are interested in modelling the rheology and relative flow behaviour (i.e. relative competence) of the kinds of rocks which occur together and form geological structures. By far the commonest lithologies from which interpretations of competence contrasts are made, are folded sedimentary and metasedimentary rocks in the psammite to pelite range. There appears to be little documentary evidence to confirm whether these lithologies generally flow as Newtonian or power-law fluids (or neither). However, studies of wavelength–thickness relationships and strain in single-layer folds in limestones (Fletcher 1974, Hudleston & Holst 1984), compared to theoretical values for Newtonian and power-law materials, suggest power-law flow for these limestones, with exponent, n, significantly greater than unity.

We remain uncertain about the extrapolation of analogue experimental data to natural deforming rocks, or how far the above analyses for limestones can be taken as indicative of other rock types. If rocks do generally flow as power-law fluids, we are faced with an endless range of theoretical permutations, when the possible variations of A and n for two adjacent layers are considered. Until these questions are better resolved, we consider it justified to model competence contrast using Newtonian rheology, for both theory and experiments.

Strain refraction across competence contrasts

Treagus (1973, 1981a, 1983, 1988) has examined theoretical variations of stress and strain across layers of different viscosity, with the aim of quantifying the expected strain variations across lithological contrasts, or competence contrasts. The theoretical model assumes planar Newtonian layers which are in perfect adherence (equal interfacial stretching and equal interfacial shear stress). Treagus (1983, 1988) (Fig. 1) showed that finite strain ellipsoids would refract and change shape across viscosity contrasts, by an important rule: *the ratio of layer-parallel finite shear strain across a boundary is equal to the inverse viscosity ratio* (also Cobbold 1983). This process may be termed *strain refraction*. The implications of this strain refraction theory to cleavage refraction in rocks were considered in Treagus (1983) (see also Talbot 1983), and some broader geological implications discussed in Treagus (1988) and references therein.

In a theoretical study of the kinematics and mechanics of coherent interfaces, Cobbold (1983) showed that the finite shear strain ratio (his K) should equal the inverse material ratio for any linear materials (Hookean elastic and Newtonian viscous). For non-linear rheologies, such as Reiner–Rivlin fluids and 'power-law' fluids, Cobbold found that K was not a constant, except in certain special deformations. Thus, a theory of *finite* strain refraction in layered 'power-law' systems, which might be considered a more suitable rheological model than Newtonian, would seem to be intractable in a general sense. Instead, we shall investigate the problems through laboratory modelling.

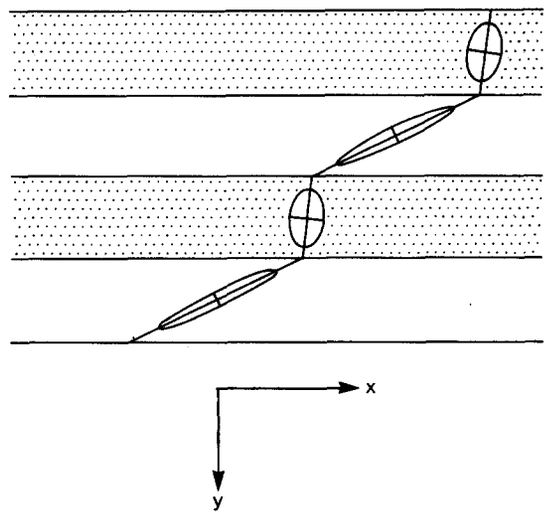

Fig. 1. Schematic pattern of strain refraction across a multilayer comprising semi-infinite planar layers of alternating Newtonian viscosity, with viscosity ratio 25. Shaded layers are the more competent. After Treagus (1983, 1988).

Laboratory modelling of strain refraction

This paper presents the results of a laboratory programme to test the theoretical rules of strain refraction and interface flow relationships. The present experiments were designed for the Hans Ramberg Tectonic Laboratory, Uppsala, using the existing calibrated modelling materials and deformation rigs. The primary purpose was to test the theoretical (Newtonian) model of strain refraction (Treagus 1983, 1988), using Newtonian laboratory materials; specifically, to test whether the shear strain ratio across a boundary is equivalent to the inverse viscosity ratio. The secondary purpose was to examine the nature of strain refraction for strain-rate dependent rheologies.

We considered two kinds of model designs in which the layers are oblique to principal displacements, and which therefore have components of layer-parallel shear strain (which might refract). The simplest is layers in layer-parallel simple shear; there is no component of layer-parallel straining in such a system, and so, in theory, the simple-shear ratio should be the inverse viscosity ratio. This is very much a 'special case' deformation, but useful to reveal processes in their simplest form. The second and more general system is one of

oblique contrasting layers in pure shear, which was the kind of set-up used in some previous experiments (Treagus 1972).

We make no attempt to scale our models to nature, for two reasons. First, these models were designed to test a working theory for strain refraction, not to model a particular natural structure, with our interest focusing more on the process, rather than exact similarity of the materials to particular rocks. Secondly, as we have attempted to show in our review of rheology and competence, the parameters for flow in rocks, and the actual flow laws, are far less from certain for ductile geological deformations of varied metasedimentary rocks.

LABORATORY MODELS, PROCEDURES AND MATERIALS

Viscometry

The viscosities of the materials used were measured in the Hans Ramberg Tectonic Laboratory at Uppsala, using two kinds of viscometers: the German Haake capillary (extrusion) viscometer, and the concentric cylinder (Couette) viscometer constructed at Uppsala by R. Häll. The functions, advantages/disadvantages and necessary corrections, particularly for non-Newtonian materials, have been discussed by Weijermars (1986a).

Rheology maps

The properties of the model materials described below are presented on a *rheology map* (Fig. 2) of log shear stress against log shear strain rate. This kind of graph is commonly used to present viscosities and flow properties of model materials (e.g. Dixon & Summers 1985, 1986, Weijermars & Schmeling 1986, fig. 3, Sokoutis 1987), and is particularly useful for distinguishing Newtonian, power-law and other types of rheologies (see Fig. 2 caption). This kind of diagram will also be used later in the paper, as a method of representing values of stress and strain rate refraction in the models and in theory.

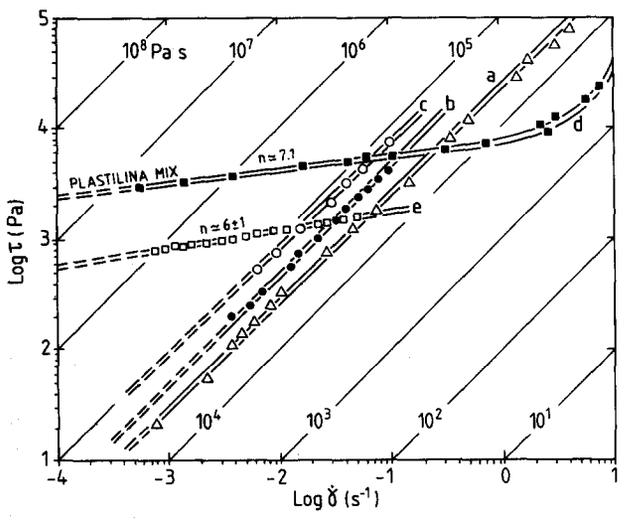

Fig. 2. Viscosity diagram and *rheology map* of log τ vs log $\dot{\gamma}$, for the materials used in this paper, taken from laboratory viscometry measurements (Table 1). τ is shear stress and $\dot{\gamma}$ engineering shear strain rate (=$2\dot{e}$, the natural strain rate). Newtonian materials follow the diagonals, which also provide the effective viscosity scale. Other straight lines indicate 'power-law' flow, with stress exponent, n, given by the cotangent of line slope. *Material a*: Rhodorsil Gomme 'bouncing putty'; *Material b*: PDMS; *Material c*: mixture of 77 wt % PDMS and 23 wt % barium sulphate; *Material d*: mixture of 67 wt % Plastilina and 33 wt % Rhodorsil Gomme; *Material e*: Dow Corning silicone putty. Materials at laboratory room temperature: see text and Table 1 for more details.

Model materials

Most of the materials used in the experiments described in this paper are silicone-based compounds which have been examined in detail by Weijermars (1986a). Two are Newtonian within the range of strain rates used, with not very different viscosity. These proved suitable for testing whether the theoretical rule that the finite shear strain ratio equals the inverse viscosity ratio for Newtonian behaviour (Cobbold 1983, Treagus 1983, 1988) is satisfied in laboratory experiments. We would have preferred to use two Newtonian silicones with a higher viscosity ratio (e.g. 5, 10 and more), but suitable materials were not available. Stiffening Newtonian silicones with fillers generally takes them away from Newtonian behaviour (Onogi & Matsumuto 1981), and so our stiffer materials such as silicone putties and various mixtures were all non-Newtonian to various degrees. They were generally shown from viscometry (see below) to be close to 'power-law' flow.

The five model materials used in the experiments are described below, and their properties are summarized in Table 1 and Fig. 2.

Material a: *Rhodorsil Gomme GSIR (RG)* is a pink opaque bouncing putty supplied by Rhone-Poulenc of Paris. The viscosity of RG was determined by the Haake steady-state extrusion viscometer as 2.9×10^4 Pa s (Sokoutis 1987). This closely matched measurements using the coaxial cylinder viscometer.

Material b: *polydimethylsiloxane polymer (PDMS)* is a transparent and colourless silicone gel manufactured by Dow Corning of Great Britain under the code name SGM 36. It is one of a group of PDMS liquid polymers investigated by Weijermars (1986b,c). We measured its viscosity in the Haake steady-state viscometer as 4.8×10^4 Pa s (Table 1).

Material c: *mixture of PDMS + $BaSO_4$*. This is a homogeneous mixture of 77 wt % of PDMS (described above) and 23 wt % barium sulphate powder. It forms an opaque pure white material. Flow measurements and viscosities using the coaxial cylinder viscometer show that it deviates only slightly from Newtonian (Fig. 2), with a power-law exponent $n = 1.1$. Its viscosity falls in the range 9.9×10^4–7.79×10^4 Pa s, for the experimental strain rates of 5×10^{-4}–10^{-2} s^{-1} used (Table 1).

Material d: *mixture of Plastilina + Rhodorsil Gomme*. This is a homogeneous mixture of 67 wt % 'Plastilina' (50% red and 50% white) with 33 wt % Rhodorsil Gomme GSIR (RG), already used and described by

Table 1. Viscosity measurements from viscometry for the five model materials used in the experiments. See also Fig. 2

Viscosity diagram	Physical model material	Temperature (°C)	Viscosity at s.s.r.* 5×10^{-4} s^{-1} (Pa s)	Viscosity at s.s.r.† 1×10^{-2} s^{-1} (Pa s)	Power law exponent n	Rheological behaviour
a	GSIR (R.G.)	24 ± 1	2.90×10^4	2.90×10^4	1.00	Newtonian
b	PDMS	22 ± 1	4.80×10^4	4.80×10^4	1.00	Newtonian
c	77%:23% (wt %)‡ PDMS:$BaSO_4$	21 ± 1	9.90×10^4	7.91×10^4	1.1	Non-Newtonian
d	67%:33% (wt %)‡ Plastilina:GSIR	24 ± 1	5.50×10^6	4.20×10^5	7.12	Non-Newtonian
e	Dow Corning 3179	23 ± 1	1.36×10^6	1.15×10^5	6 ± 1	Non-Newtonian

*s.s.r. = shear strain rate (from pure-shear apparatus).
†s.s.r. = shear strain rate (from simple-shear apparatus).
‡wt % = mixture by weight %.

Sokoutis (1987 fig. 4, material 'f') for mullion experiments. Plastilina is the Swedish version of Plasticine (see McClay 1976, Weijermars 1986a). The rheology of this mixture is summarized in Fig. 2 and Table 1, after Sokoutis (*op. cit.*).

Material e: Dow Corning Dilatant Compound No. 3179 (*DC*) is a pink silicone putty, similar in appearance to RG (see above), but distinctly different in rheology. It is a viscoplastic material in the general sense, with a complex rheology which has already been investigated by Dixon & Summers (1985, 1986). Our viscosity measurements using the coaxial cylinder viscometer differ somewhat from those of Dixon & Summers (1986, fig. 1) (Fig. 2). We similarly find that within the strain rates 10^{-4}–10^{-2} s^{-1}, DC is approximately a power-law fluid in the range $n = 6 \pm 1$ (Dixon & Summers have 7 ± 2), but our effective viscosities at strain rates of 5×10^{-4} and 10^{-2} are 1.36×10^6 and 1.15×10^5 Pa s, respectively, at 23° ± 1°: about twice the values predicted by Dixon & Summers (1986, fig. 1). A possible explanation is that during manufacture considerable variations in physical properties arise, so that different batches could be measurably different. Our values are consistent with the strain refraction results described later. The question of whether DC behaves approximately as a Bingham body over a wide range of strain rates (Dixon & Summers 1986) need not concern us here, as our experiments fall within the range of strain rates (10^{-4}–10^{-2}) where their results and ours are consistent with power-law flow.

Experimental design

Simple-shear experiments. The simple-shear box has a standard design, and is described in detail by Arnbom (1976). All the experiments were deformed at the slowest strain rate for this shear box, which is $\dot{\gamma} = 10^{-2}$ s^{-1}. This is the bulk shear strain rate, but individual layers or regions of the box deform at very different rates, which is the subject of this paper.

In the main simple shear experiments, a single layer of contrasting viscosity was placed parallel to the shearing direction of the box (Fig. 3a). The layer was not intended to rotate during deformation, nor stretch or shorten.

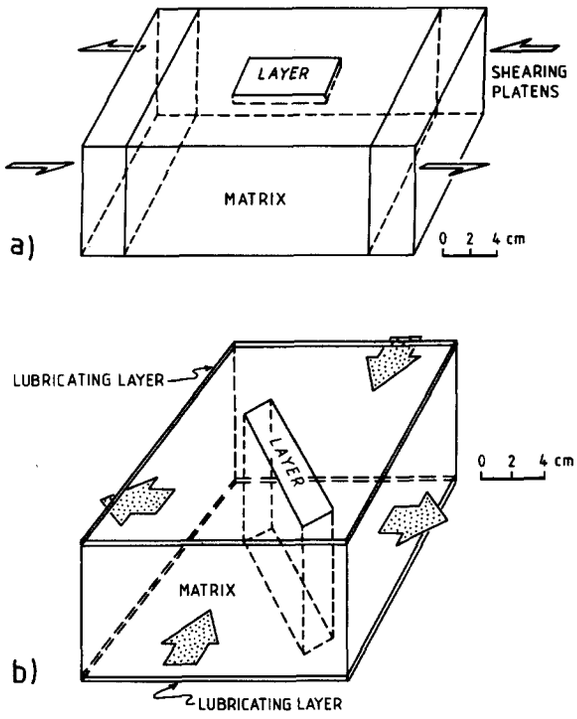

Fig. 3. Schematic experimental designs for (a) simple-shear and (b) pure-shear models. See text for details of individual experiments.

The single layers were made to the dimensions of a perspex strip, 5 × 2.5 × 0.8 cm. The strip was pressed into the matrix to make a rectangular parallelepiped mould for the layer, and the layer carefully laid in place. Thus, these layers effectively 'floated' in the confining medium (Fig. 3a), so as to avoid them being driven by the base plates of the box (i.e. at the box strain rate). The layers were thus able to deform at a different rate from the box and the confining medium, as will be described.

The confining matrix material was either the pink Rhodorsil Gomme (RG) or the colourless PDMS, both of which are shown to be Newtonian in the range of strain rates used. The former material was more satisfactory for photographing.

Two additional types of simple-shear experiment were constructed. (1) 'Half and half' experiments comprise a shear box half filled with one material, and half a contrasting material, with a vertical interface parallel to the shear direction. This is designed to test the relative

effects of boundary refraction which, by definition, induce heterogeneous strain patterns, compared to the requirement that the box must deform to the bulk rate. (2) One multilayer experiment was constructed to compare the features of refraction in a repeated rather than isolated contrasting layer. For both these experiments, the material boundaries were the full width and depth of the simple-shear box, unlike the single-layer experiments.

All these experiments were marked with a fine grid of lines parallel and perpendicular (initially) to the interfaces, as described later.

Pure-shear experiments. A few pure-shear experiments were conducted, using the pure-shear apparatus described in Sokoutis (1987, appendix). These mostly proved far more difficult to construct than the simple-shear models, and presented several problems of measurement and analysis. Unlike the simple-shear apparatus which has a constant $\dot{\gamma}$, the pure-shear box does not have a constant natural strain rate, $\dot{e}$, (where $\dot{\gamma} = 2\dot{e}$) (Sokoutis 1987, fig. 5), but increases with increased bulk shortening (i.e. the shortening velocity is constant). We take a mean value of $5 \times 10^{-4}\,s^{-1}$ for $\dot{\gamma}$, for descriptive and illustrative purposes. However, as we shall explain later, our inability to compute the exact strain rate in different parts of these models prevents us using the results of pure shear experiments, quantitatively, for the strain-rate dependent materials used here.

The models were assembled in a number of stages, according to the design in Fig. 3(b). It was necessary for the confining matrix to be a solid-plastic material, rather than Newtonian; Dow Corning 3179 (DC) was used. The matrix block was cut diagonally at the required angle for the oblique layer (30° or 60°), which was then inserted. The assembly was placed in the pure-shear box over a thin lubricating base layer of PDMS, and marked with a grid (see below). The second lubricating layer of PDMS was placed over this, coated with glycerol, and the confining top plates finally fixed.

The marker grids

A marker grid of orthogonal lines was placed on the free horizontal surface of each model (e.g. Figs. 5–8), with one set of gridlines parallel to the layer. The layer-perpendicular set when deformed gave an immediate measure of the layer-parallel shear strain, and the shear strain ratio across viscosity boundaries. The fine carbon grids were produced according to the 'photocopy' method of Dixon & Summers (1985, p. 93), with a modification that it proved more useful to use transparent (acetate) sheets, rather than paper.

Measurements from models

Measurements were made from the model photographs for each stage of deformation. A central initially layer-normal grid-line (G) was chosen, and measurements made of its shear strain throughout deformation

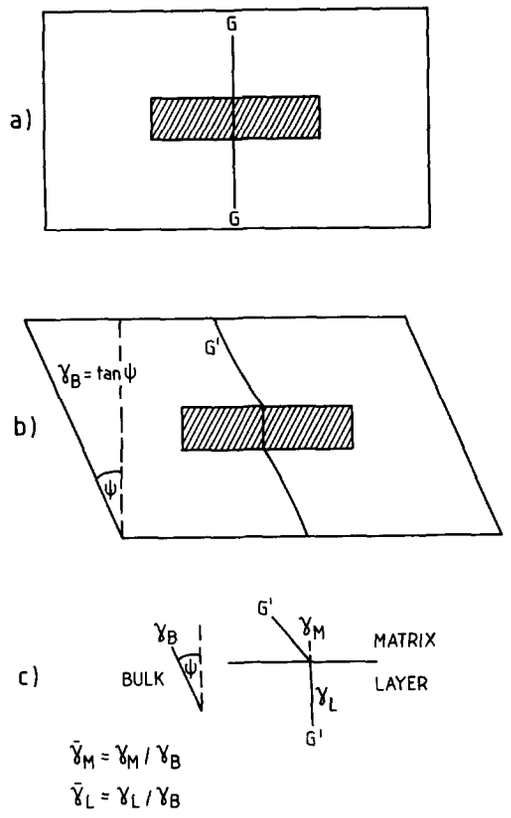

Fig. 4. Model measurements and their definitions, for a typical single-layer simple-shear model. (a) G is an initial central (layer-normal) grid-line, which (b) deforms to the G′ trajectory, after bulk angular shear ψ. (c) Enlargement of the matrix–layer boundary, showing the γ definitions. In this schematic example, the layer is more competent than its matrix.

(Fig. 4). As will be described later, this deformed grid-line (G′) is generally curved, showing a smooth gradient in the matrix but sharp refraction at the matrix–layer boundary (Fig. 4b). This refraction is measured by the boundary *finite shear strain ratio*, γ_M/γ_L ($=K$) (Fig. 4c), which will be compared to the inverse viscosity ratio (η_L/η_M) (Cobbold 1983, Treagus 1983, 1988).

The smooth gradients of shear strain towards a viscosity boundary are most conveniently measured as *normalized shear strains*, $\bar{\gamma}$, defined as the ratio of the finite shear strain, γ, to the bulk (or box) shear strain (termed γ_B). $\bar{\gamma}$ provides a useful expression of the strain intensification, or depletion, at (or approaching) a viscosity boundary, as a factor of the bulk shear strain. In particular, we shall determine the normalized matrix boundary shear strain, $\bar{\gamma}_M$ (Fig. 4c), to see whether this seems to be a constant for the model (i.e. a material property) or depends on the box strain. Normalized values as factors of the bulk/box value are also a convenient way of expressing local shear strain *rates* as a function of the bulk shear strain rate.

All angular measurements are considered to be accurate within ±1°. A constant error range cannot be assigned to the shear strains and shear strain ratios, as the error of ±1° clearly has a more significant effect on tangent values of small angular shears than large angles, and thus a greater potential error for ratios like K.

Table 2. Laboratory models, their specifications and summary measurements. Shear strain nomenclature is defined in Fig. 4; material codes are given in the text (also Table 1 and Fig. 2). Predicted K values (right columns) are explained in the Discussion and Fig. 15

Fig. No. (photos)	Model No. type	Layer material	Matrix material	Viscosity ratio $m = \eta_L/\eta_M$ from Table 1	Measured $K = \gamma_M/\gamma_L$	$\bar{\gamma}_M$ mean value	$\bar{\gamma}_L$ mean value	$\alpha = h_M/h_L$	Predicted K for linear τ_x	
									Exact	Approx.
Fig. 5(a)	SR-2 SLSS	PDMS	GSIR	1.66	1.53	1.21	0.790	2.56	1.71	1.65
Fig. 5(b)	SR-8 SLSS	GSIR	PDMS	0.60	0.68	0.83	1.220	2.56	0.65	0.68
—	SR-6 SLSS	PDMS/B	PDMS	1.65–2.06	1.90	1.35	0.700	2.70	2.68	2.55
Fig. 6(a)	SR-7 SLSS	DC-3179	PDMS	28.3*	29.5	1.47	0.050	4.0–4.05	25.5–34.3	24.5–32.7
Fig. 6(b)	H + H SS	Half model with GSIR and half with DC-3179		62.0*	63.0	2.50	0.038			
Fig. 7	MLSS	GSIR (2)	DC-3179 (3)	Indeterminate						
Fig. 8(a)	R-1 SLPS	P/GSIR	DC-3179	Highly variable for model						
Fig. 8(b)	R-2 SLPS	P/GSIR	DC-3179	Highly variable for model						

Key: SL = single layer; ML = multilayer; H + H = 'half and half'; SS = simple shear; PS = pure shear. (2) and (3) indicate number of layers.
* is a viscosity ratio computed for the particular model strain rates, and is not a material constant.

RESULTS FOR INDIVIDUAL MODELS

Single layers in simple shear

The results of four experiments will be described in detail, with the specifications and summary results given in Table 2.

Model SR2: PDMS layer in RG matrix. This model experiment is illustrated in Fig. 5(a). The clear PDMS layer is slightly stiffer than the RG host. At all stages of deformation, the grid can be seen to refract slightly at the boundary, with a smaller angular shear in the layer than either the bulk shear or the matrix boundary shear.

Model measurements are shown in Fig. 9 (summarized in Table 2). The boundary shear strains are graphed in Fig. 9(a), and it is apparent that the shear strain ratio, K (RG/PDMS), is independent of the bulk shear strain, falling in the range 1.43–1.6, with the average for model stages 4–9 as 1.53. This is quite close to the viscosity ratio of PDMS/RG of 1.66 from viscometry (Table 1), particularly given the uncertain error bars on this ratio and the K measurements.

The normalized matrix boundary shear strain ($\bar{\gamma}_M$, Fig. 4) falls in the range 1.12–1.28 (average 1.21) (Fig. 9c). It is a 'strain intensification' which shows no systematic change throughout model deformation, so it appears to be a material property, and thus a potential predictor of the boundary viscosity ratio (see Discussion).

Model SR8: RG layer in PDMS matrix. This model was designed to be the exact inverse of model SR2 above, where now the layer is the less stiff material. Stages of the deformation are shown in Fig. 5(b), and all show refraction of the grid across the boundary. In this experiment the layer has a larger angular shear than either the bulk shear or the matrix boundary shear.

Model measurements are given in Fig. 9(b) (summarized in Table 2). The boundary shear strain ratio, K (PDMS/RG), falls in the range 0.65–0.71, with an average of 0.68. For comparison with SR2, the reciprocal values of these are 1.41–1.53 (average 1.47), which are similar to SR2, though slightly less. This experiment also shows no systematic trend of the ratio with bulk shear strain, supporting an interpretation that this is a material constant. Like SR2, the value is lower than the 1.66 from viscometry (Table 1, Fig. 2).

The normalized matrix boundary shear strain ($\bar{\gamma}_M$) for this experiment is a 'strain depletion' with values in the range 0.81–0.84 (average 0.83) (Fig. 9c, Table 2). This boundary depletion factor appears to be a material property independent of the degree of deformation, and the close agreement between the reciprocal of 0.83 (=1.20) and the comparable value for model SR2 (1.21) confirms this conclusion.

Model SR6: PDMS + $BaSO_4$ mixture layer in PDMS matrix. This model (not illustrated) has a layer of material c, which is slightly stiffer than the matrix and is slightly non-Newtonian (Fig. 2, Tables 1 and 2). The boundary γ ratio, K (matrix:layer), was measured for four model stages as 1.83–2.00 (average 1.90). The viscosity ratio from the viscometry measurements is not a constant for these materials, but is dependent on the strain rate in the layer (Table 2), which is slightly less than the bulk shear strain rate (*ca* 7×10^{-3} s^{-1}); from Fig. 2, this gives a viscosity ratio of approximately 1.7. Given the close agreement of the K values at different bulk shear strains, it seems reasonable to suggest that the K value of 1.9 gives the viscosity ratio of these materials more accurately than the laboratory viscometry.

Model SR7: DC layer in PDMS matrix. This (Fig. 6a) is the only simple-shear experiment which will be pre-

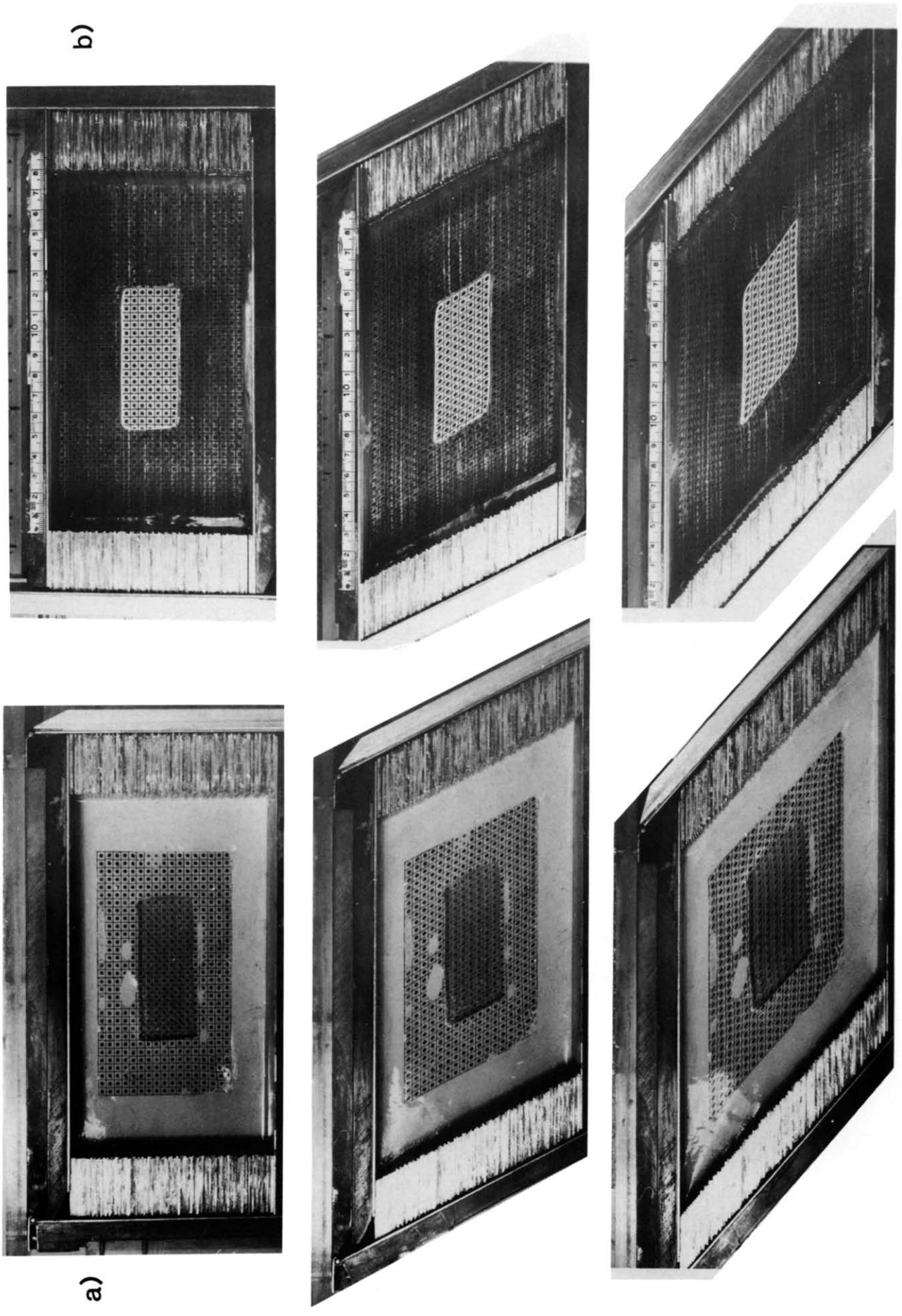

Fig. 5. Two reciprocal simple-shear models, same scale (cm ruler). (a) SR2, a PDMS layer in an RG matrix, at model stage 1 ($\gamma_B = 0$), stage 5 ($\gamma_B = 0.55$) and stage 8 ($\gamma_B = 1.12$). (b) SR8, with RG layer in PDMS matrix, at model stages 1 ($\gamma_B = 0$), 6 ($\gamma_B = 0.55$) and 9 ($\gamma_B = 1.15$). Model details and measurements in Table 2 and Fig. 9.

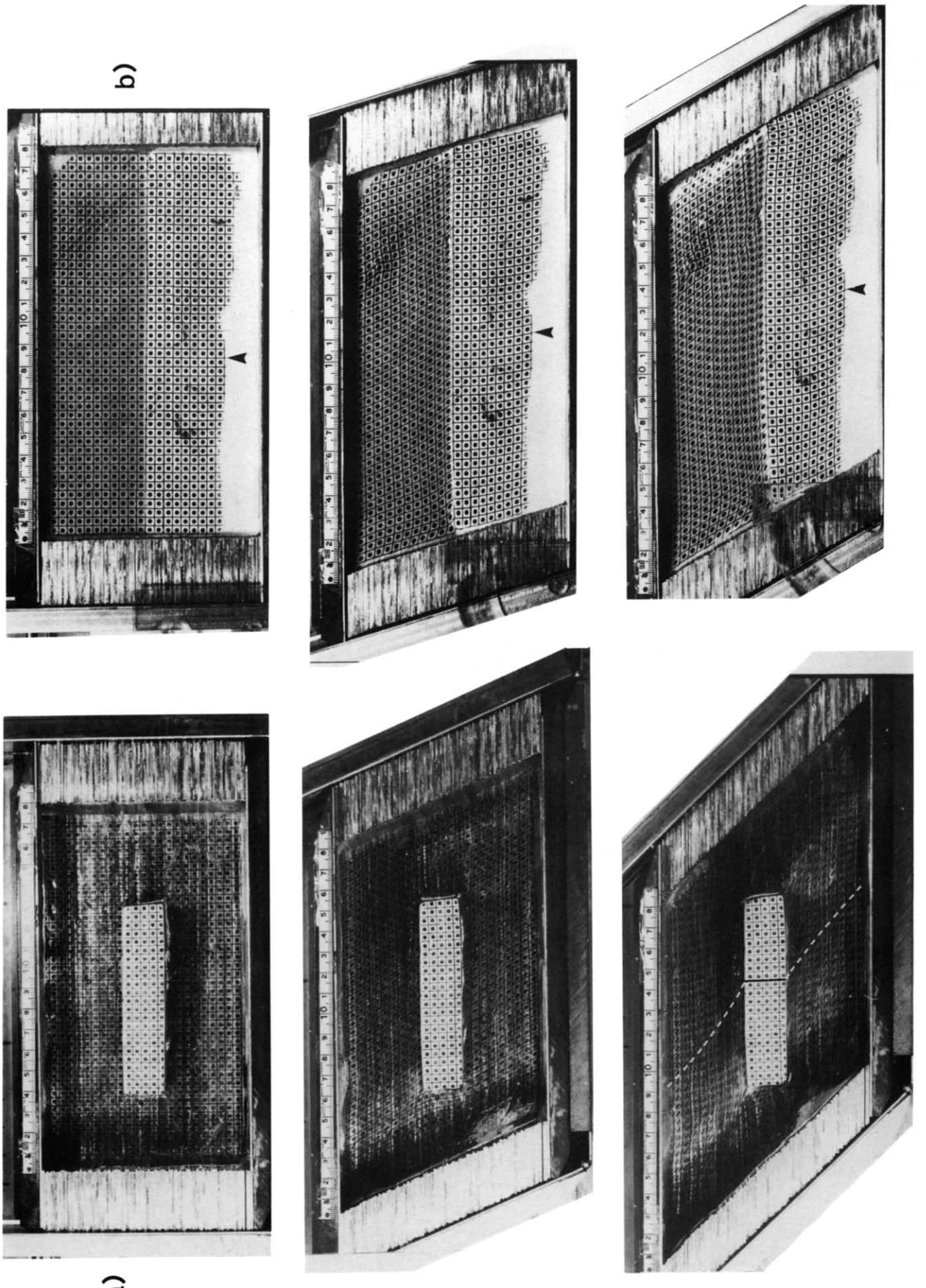

Fig. 6. (a) Model SR7, a DC layer in PDMS matrix, at model stages 1 ($\gamma_B = 0$), 5 ($\gamma_B = 0.4$) and 8 ($\gamma_B = 0.93$). Refraction highlighted for last stage. Model measurements in Fig. 10. (b) 'Half and half' model; upper half RG, lower half DC. Model stages 1 ($\gamma_B = 0$), 4 ($\gamma_B = 0.32$) and 8 ($\gamma_B = 0.58$). Measurements for the arrowed grid-line in Fig. 11.

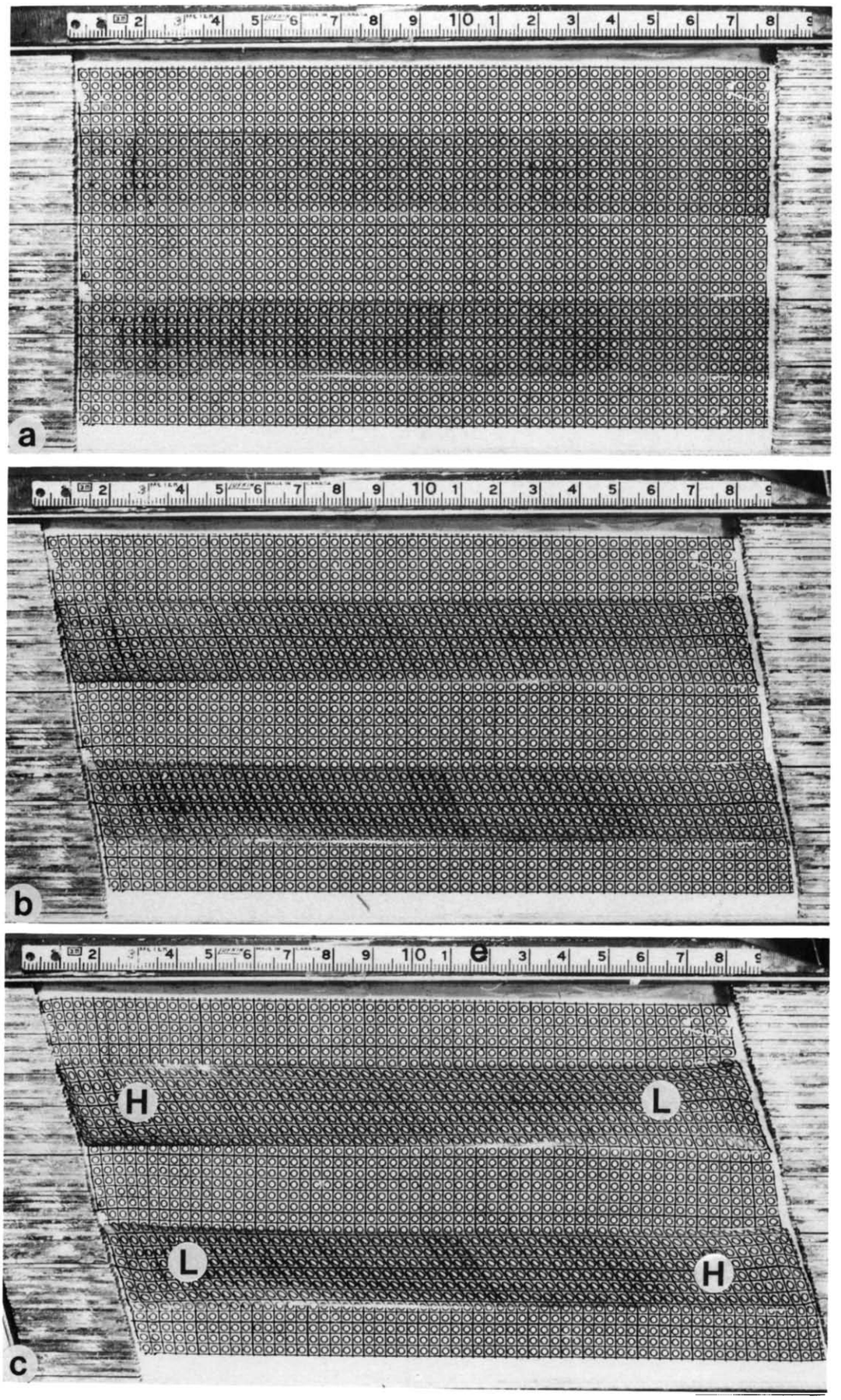

Fig. 7. Multilayer model in simple shear. Layers from top to bottom are DC, RG, DC, RG and DC. (a) $\gamma_B = 0$, (b) $\gamma_B = 0.18$ and (c) $\gamma_B = 0.31$. The positions labelled H and L are 'highs' and 'lows' of the model surface which indicate marked departures from plane strain.

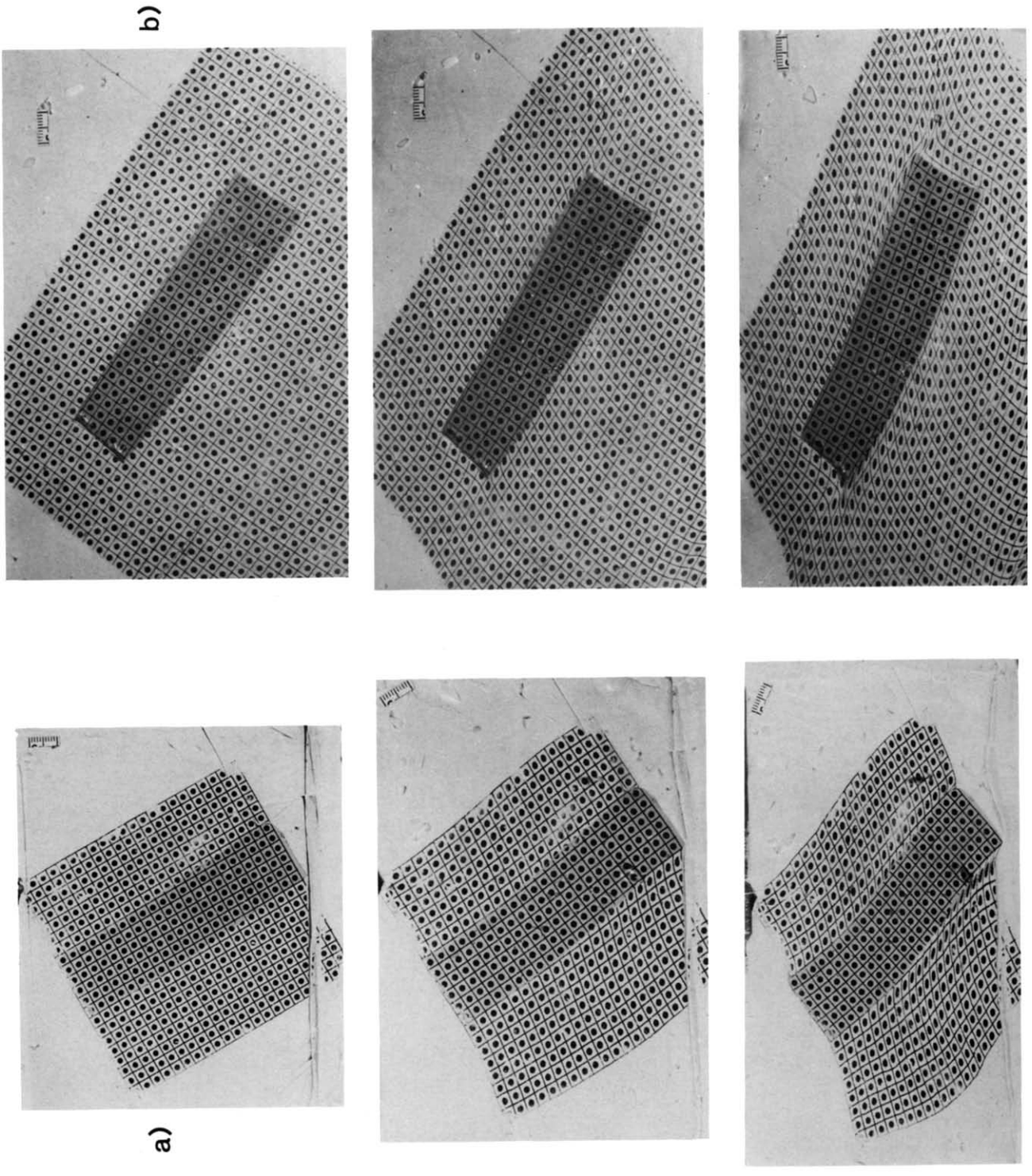

Fig. 8. Pure-shear models, according to the design in Fig. 3(b). Layer is Plastilina mixture and matrix DC; scale bar is 1 cm. (a) Model R1, layer at 30° to principal shortening. (b) Model R2 at 60° to shortening. (a) and (b) show model stages at 0, 8 and 21% bulk shortening. Note the strongly heterogeneous strain patterns in and around the layers, compared to the simple-shear experiments.

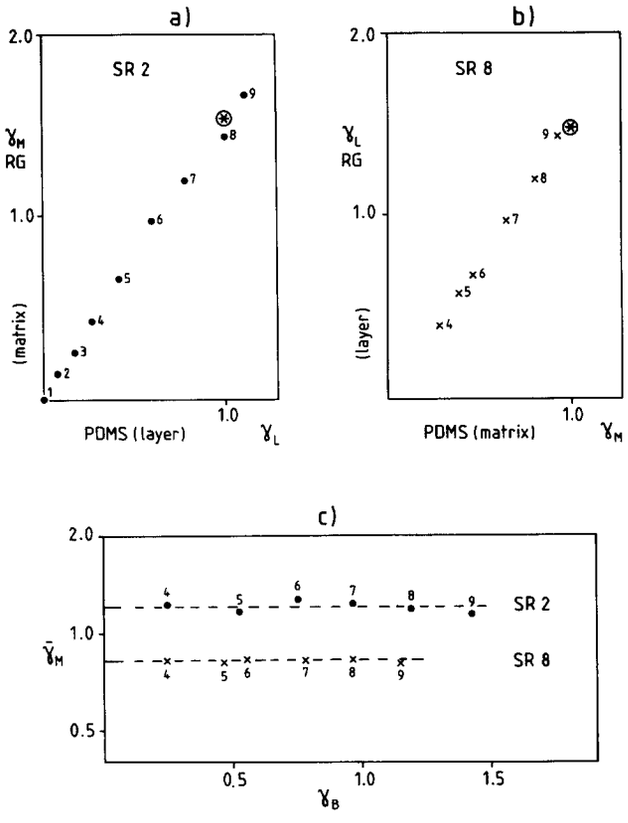

Fig. 9. γ measurements for models SR2 and SR8 (Fig. 5), according to the definitions in Fig. 4. Numbered points are model stages at increasing γ_B. (a) and (b) are γ_L vs γ_M curves for SR2 and SR8, standardized for comparison (RG vs PDMS). Note the similarity. Circled stars are the computed average shear strain ratios of 1.53 for (a) and 1.47 for (b). (c) $\bar{\gamma}_M$ values vs bulk shear strain, γ_B (see Fig. 4) for SR2 (dots) and SR8 (crosses) on a log scale for $\bar{\gamma}_M$, to show their closeness to reciprocality. The broken lines indicate the mean value for each model, and illustrate the independence of $\bar{\gamma}_M$ values with bulk strain.

sented in detail, which uses a layer of markedly non-Newtonian material. The boundary shear strain ratios (K) are in the range 26.5–31.5, with a mean of 29.5 (Fig. 10a, Table 2), with no systematic variation with bulk shear strain. The normalized matrix boundary shear strain ($\bar{\gamma}_M$) ranges from 1.43 to 1.49 (mean 1.47, Table 2). This means that the shear strain in the matrix in the zone adjacent to the DC layer is almost 50% more than the bulk (box) shear strain, a considerable intensification factor. In contrast, the normalized layer shear strain ($\bar{\gamma}_L$; Fig. 4c) is measured to be 0.045–0.056 (0.05 in Table 2); i.e. *ca* 1/20 the bulk shear rate. These normalized strain factors, like the shear strain ratio, K, seem to be material properties, independent of the bulk shear strain (Fig. 10b).

Recall that the DC layer does not have a constant viscosity, so we need to know its strain rate to determine its viscosity from Fig. 2. The value of $\bar{\gamma}_L = 0.05$ means a layer shear strain rate of 0.05 × box rate throughout the model deformation; i.e. $\dot{\gamma} = 5 \times 10^{-4}\,s^{-1}$ (coincidentally the pure-shear strain rate, Table 1). For this strain rate, the viscosity of DC is found to be 1.36×10^6 Pa s (see Fig. 2 and also Fig. 12a, explained later). As stated before, the viscosity of PDMS is 4.8×10^4 Pa s. Thus, the inverse viscosity ratio for this experiment is 136/4.8 = 28.3. This value is within the range of measured K values given above (Fig. 10a) and so we are confident that the strain refraction in this experiment is a measure of the viscosity ratio. However, this ratio of 28–29 is specific to the experiment, and cannot be considered as a general viscosity ratio for DC/PDMS.

This model provides a good example of strain variation in the matrix (Fig. 6a), from the bulk shear strain at the box edge to a considerably higher strain adjacent to the layer. Shear strain profiles are given in Fig. 10(b), for four model stages. The normalized shear strain values, $\bar{\gamma}$, showed no significant difference between the different stages, but a consistent pattern (as Fig. 10c), suggesting a specific strain-intensification factor for this model. It is a slightly sinuous trend about a broadly linear increase in $\bar{\gamma}$ towards the layer edge. Whether normalized γ values should be expected to be linear or not will be addressed in the Discussion.

Simple-shear 'half and half' experiment

Figure 6(b) shows a model in simple shear that comprises two halves: a weaker (Newtonian) Rhodorsil Gomme (RG) half (above), and a stiffer non-Newtonian DC half (below). This model was designed to test the degree to which the bulk shear strain of the shear box controls the strain variation, and how refraction at a material interface can be accommodated within a bulk simple-shear deformation. It is evident in Fig. 6(b) that the dramatic strain refraction in the central part of the box gives rise to necessary patterns of heterogeneous strain towards the edge, and departures from simple shear. As deformation proceeds, two features progressively become pronounced: (i) the interface bends, even though it was initially parallel to the simple shearing direction, and (ii) topographic 'highs' and 'lows' develop on the free surface, indicating local departures from plane strain. The full patterns of heterogeneous strain have not been analysed, but shear strains across a central grid line (arrowed in Fig. 6b) have been measured and normalized. Measurements were restricted to the earlier stages of deformation, before the two accommodation features became too pronounced.

Figure 11(a) shows values of γ across the box, for four stages of deformation. The normalized values show a similar pattern for each stage, which, like the experiments described above, supports the conclusion that the intensification or depletion factors are properties of the materials and the model. Figure 11(b) shows the average normalized shear strain trend across the box, for the Newtonian RG and the power-law DC halves. These trends will be discussed later.

The boundary shear strain ratio, K, has a value of 63 (taken as the ratio of the average normalized boundary strains of 2.5 and 0.038, from Fig. 11b). The ratios for individual model stages have a wide range, probably due to the large errors in the tangents of small angles with an error range of ±1°, which is the reason we prefer to use the average normalized ratio. Comparing our value of $K = 63$ to the inverse viscosity ratio for the experiment

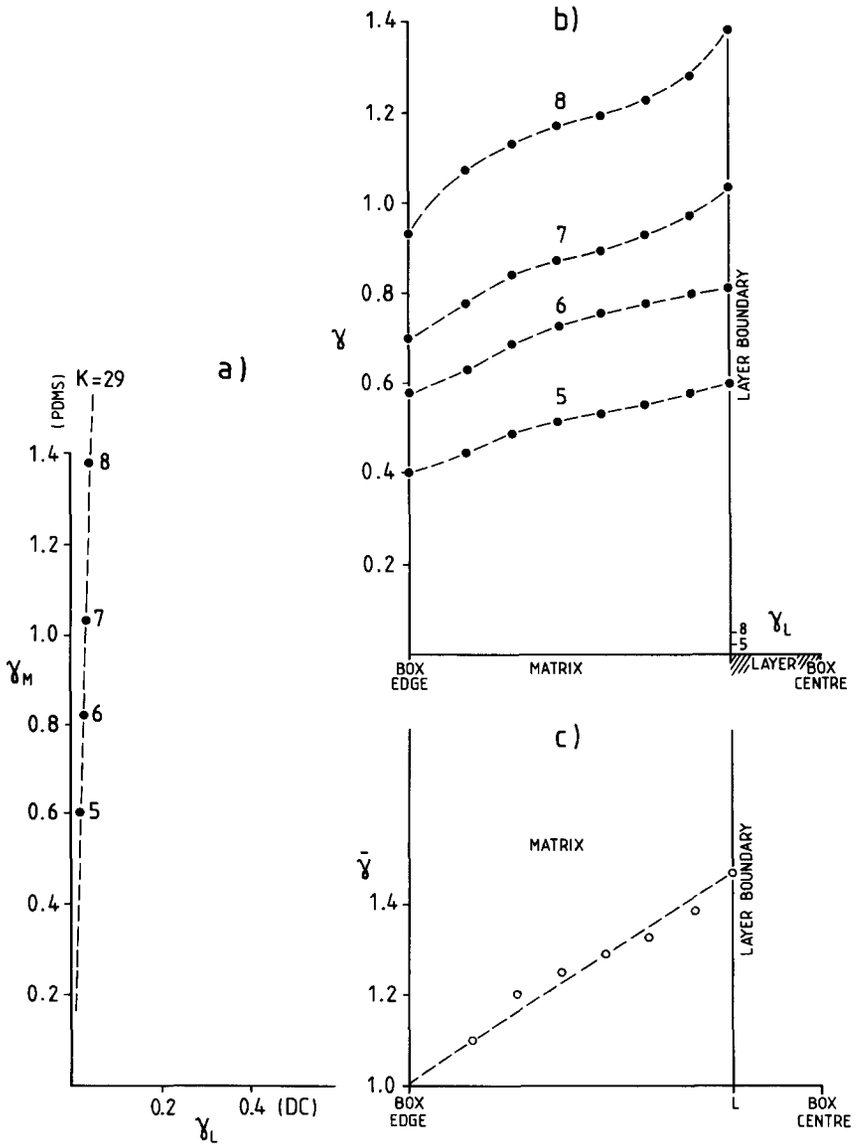

Fig. 10. γ measurements for model SR7 (Fig. 6a). (a) γ_L vs γ_M, showing no consistent change in K ($=\gamma_M/\gamma_L$) with increasing bulk strain (stages 5–8). (b) γ values across the shear box, from edge to centre. (c) $\bar{\gamma}$ values computed and averaged from (b) (stages 5–8).

using the viscometry data (Table 1 and Fig. 2), we have the viscosity of RG = 2.9×10^{-4} Pa s, and derive a value for DC of *ca* 1.8×10^{6} Pa s, for the strain rate of 3.8×10^{-4} s^{-1} (from Fig. 2). This gives a ratio of 62, which is remarkably close to our mean K.

Multilayers in simple shear

The experiment consists of five layers of alternating DC and RG (Fig. 7), deformed in layer-parallel simple shear. The pattern of shear strain refraction is shown by the sharp grid refraction from layer to layer, and the clear difference between the strain ellipses in the two layer types. Note that these are the same two materials as the 'half and half' model in Fig. 6(b).

The shear strain in the DC layers away from the driving edges of the box are too small to measure, and therefore we cannot compute the shear strain ratio, K, nor the shear strain rate and effective viscosity for DC. All we can say is that these layers deformed at a very small strain rate, to the left of the rheological field shown for DC in Fig. 2. This illustrates, again, that viscosity ratio is model specific and not easily predicted before an experiment, or from another model (e.g. the previous 'half and half' model).

Figure 7 illustrates some important features of this multilayer model, which are not produced in the single-layer experiments.

(1) The refracted grid lines (the γ trajectories) remain close to straight within each layer, and then refract sharply across interfaces. This is closer to the theoretical strain refraction pattern of Treagus (1983, 1988) shown in Fig. 1, than to the results for the shorter and single layers described above.

(2) The layers in this model were constructed right up to the shearing edge of the box, rather than made to be central inclusions like Fig. 3(a). At the driving box edges, these layers must therefore deform at the box rate, but only a slight distance away, the two layers deform very differently.

(3) The outermost layers are of the stiffer (DC) material. It appears that only a narrow strip of these layers deforms at the box rate (unfortunately not grid-marked); we might have expected a smoother transition from the box strain to almost zero strain, and smoothly curved trajectories, in these outer layers.

(4) The incompetent RG layers show about twice the shear strain of the bulk values. This is a clear example of strain partitioning (Lister & Williams 1983) between competent and incompetent layers.

Like the 'half and half' model, this experiment developed patterns of strongly heterogeneous strain caused by accommodation of refracting strains within the bulk simple shear. Surface topographic 'highs' and 'lows' developed at higher strains (Fig. 7c), as the strains noticeably departed from plane strain.

Single layers in pure shear

Two experiments will be described which have an oblique layer of Plastilina mixture (67% wt Plastilina, 33% Rhodorsil Gomme) in a matrix of Dow Corning (DC). Model R1 has the layer at 30° to the principal shortening direction (Fig. 8a), and Model R2 at 60° (Fig. 8b), both constructed as described earlier (see Fig. 3b). Both layer and matrix are non-Newtonian materials (Fig. 2 and Table 1), which are approximately 'power-law' at these deformation rates (discussed earlier).

Both models exhibit clear strain refraction (Fig. 8), but this is difficult to quantify and compare with viscosity ratio measurements, for the following reasons.

(1) Neither model began with a perfectly straight layer of uniform thickness, and the grid was therefore not exactly parallel to the layer, along its length.

(2) Deformation within the box was strongly heterogeneous, both within the matrix and along the central layer. This heterogeneity was partly due to external boundary conditions, and partly because the 'layer' was actually a rectangular inclusion.

(3) Local variations of finite strain in the matrix and layer indicate that there was considerable strain rate variation between different points in the model. The effective viscosities of layer and matrix can only be determined from Fig. 2 from knowledge of these strain

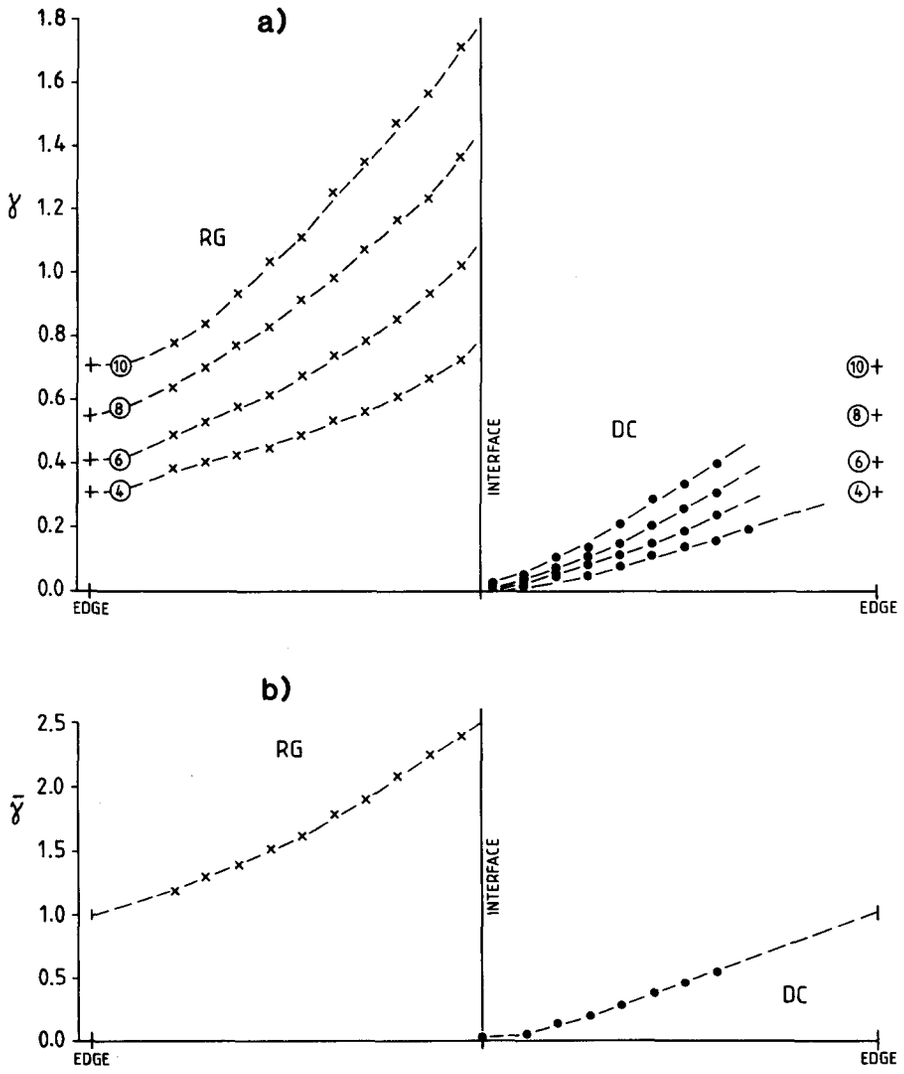

Fig 11. γ measurements for the 'half and half' model (Fig. 6b). (a) γ values along the central grid-line marked in Fig. 6(b), for four model stages (4, 6, 8 and 10). The γ_B values for each are given by the left and right values of the graph (crosses); the box edges. (b) Average normalized γ profiles ($\bar{\gamma}$), from (a). Note that this is not exactly linear in RG or DC.

rates (where normal natural strain rate, $\dot{e}$, for pure shear converts to engineering strain rate, $\dot{\gamma}$, by $\dot{\gamma} = 2\dot{e}$). We cannot compute these variable strain rates with sufficient accuracy to justify comparison of K and viscosity ratio.

DISCUSSION OF FEATURES OF THE MODELS

Boundary shear strain ratio and viscosity ratio

The main purpose of the model experiments was to test the rule of shear strain refraction which was fundamental to theoretical modelling of strain refraction in Treagus (1983, 1988). That is, for the models using Newtonian materials, *is the shear strain ratio equivalent to the inverse viscosity ratio*? Leading from this, can we relate the shear strain ratio to an effective viscosity ratio for the non-Newtonian model materials? Cobbold (1983) showed that the finite shear strain ratio was only equal to the inverse viscosity ratio across a coherent interface for linear rheologies (Hookean, Newtonian); for non-linear flow laws, no such finite relationship exists. However, he showed that for power-law flow, there are only two types of motion for which K equals the inverse viscosity ratio: zero shearing parallel to the interface, and simple shearing parallel to the interface. Our experiments (except for the pure shear set) fall into the second category, so will allow this relationship to be tested.

Only two experiments (SR2 and SR8) fulfil the condition that both model materials are Newtonian. These are the reciprocal pair of experiments (Fig. 5) using materials of quite similar viscosity (RG and PDMS). The shear strain ratios, K (RG/PDMS), of the two experiments (Figs. 9 and 10) are very close, but slightly less than the viscosity ratio from laboratory viscometry measurements. We cannot comment with certainty which is the more accurate measurement of viscosity ratio, as both viscometry and model measurements carry errors. However, we believe that if the shear strain ratio can be measured across material boundaries, this provides the best *immediate* measure of viscosity ratio for an experiment. Viscometry requires a considerable amount of laboratory time, and careful reproduction of model strain rates, temperature, humidity, etc. However, the disadvantage of using the shear strain ratio as a means of determining the viscosity ratio is that it is only a measure of relative viscosities, not absolute values and dimensions.

Now consider the non-Newtonian models. For all the experiments in simple shear, whether single layers or the multilayer or 'half and half' design, we found that the shear strain ratios, K, were independent of the stage of deformation, so we concluded that these were *model constants* (e.g. Figs. 9a & b and 10a). However, these K values can only measure the inverse viscosity ratio for a specific model, rather than for the materials in general. This is demonstrated by the K value for a RG–DC boundary; in the 'half and half' experiment this was 63, and in the multilayer experiment it was too large to measure (i.e. γ too small to measure in the DC layers). So we cannot predict these ratios for a particular experiment, in advance. It would be incorrect to use the *bulk* strain rate in conjunction with a rheology map such as Fig. 2 to determine effective viscosities in non-Newtonian materials, as these are deforming at quite different rates.

This, then, is the fundamental problem with all model experiments using non-linear ductile materials. The effective viscosity of the material can only be computed *after* the experiment, by computing the material's strain rate (from a grid), and then reading the viscosity from a rheology map like Fig. 2. For example, there is no means of determining the effective viscosity of the layer in model SR7 before the model is deformed; all that is known (or expected) is that the DC layer will not have the viscosity of 10^5 Pa s predicted for the box strain rate (from Fig. 2), but a considerably higher value.

There is an additional problem in determining the viscosity of non-Newtonian materials in experiments. They can only be computed if the material strain rate is constant throughout the experiment. For the pure-shear experiments, the bulk strain rate is not constant but increases, and the local strain rates are probably even more variable because of the complex patterns of strain developed. So the materials in these experiments (e.g. Fig. 8) cannot be considered to have a fixed, and therefore measurable, viscosity during the deformation.

We conclude that our experiments provide good evidence to equate the finite shear strain ratio across an interface with the inverse *effective viscosity ratio* for the power-law materials, so long as they have deformed by simple shear *at a constant rate* parallel to the interface. This supports the special case given by Cobbold (1983), although he did not specify constant simple-shear strain rate. Ongoing work suggests that this relationship can be broadened to a finite simple shearing at a non-steady rate, when the power-law materials have the same stress exponent, n.

Patterns of strain refraction

The variation and refraction of strain in these experiments does not exactly follow the pattern of sharp strain refraction shown in Fig. 1, based on theoretical modelling (Treagus 1983, 1988). This theory assumed infinite planar layers, and each particular layer in homogeneous strain, so that the only strain variations were the sharp boundary refractions. Laboratory modelling of such an ideal system is handicapped by model constraints: the finite size of the layers; the limits of model size; and problems in assembling planar layers of ductile (ideally Newtonian) material with sufficient thickness to allow accurate strain measurement.

All the models presented above illustrate sharp strain refraction across material boundaries, but they also illustrate smooth strain gradients in the matrix not included in the theoretical models. These strain gradients, seen in the curving grid lines, provide information

on compatible fields of heterogeneous strain associated with viscosity contrasts, which will be discussed in a later section.

The finite strain patterns in the models are indicated by the deformed grids. Since the models (except Fig. 8) were in simple shear, the orientation and degree of strain can be calculated simply from the γ values, from the following relationships (Ramsay 1980, Treagus 1981b):

$$\tan 2\theta' = 2/\gamma \quad (1)$$

$$X = \cot \theta' \quad (2)$$

and

$$Z = \tan \theta', \quad (3)$$

where X and Z are the principal stretch ellipse axes ($X > Z$), and θ' is the orientation of X to the simple shear direction. For a boundary refraction from matrix (M) to layer (L), given by

$$K = \gamma_M/\gamma_L \quad (4)$$

it follows that

$$K = \tan 2\theta'_L/\tan 2\theta'_M. \quad (5)$$

As K is equivalent to the inverse viscosity ratio (η_L/η_M) for Newtonian or power-law materials in steady simple shear parallel to layering, so

$$\eta_L/\eta_M = \tan 2\theta'_L/\tan 2\theta'_M. \quad (6)$$

This relationship between viscosity ratio and finite strain refraction in simple shear is identical to the general two-dimensional *stress* refraction equation in Treagus (1973).

Simple-shear strain refraction disallows θ' angles of >45°, and so cannot give rise to the kinds of strain refraction patterns illustrated in Treagus (1983) which arise from layer-parallel stretch components as well as shear components. Consequently, it is not appropriate to compare the strain refraction patterns in the present models with the examples of theoretical strain refraction in Treagus (1983, 1988) (e.g. Fig. 1), which are qualitatively similar to cleavage refraction and fanning patterns in folded rocks.

Strain refraction on rheology maps

Another special feature of the simple-shear experiments is that the results can be represented directly on a log shear stress vs log shear strain rate rheology map, like Fig. 2. This graph represents stress vs strain rate in terms of maximum shear stress and shear strain rate, and so for simple shear the graph co-ordinates are the simple-shear stress and strain rate. Application of this graph to other deformations is the subject of current work.

Figure 12(a) summarizes the results of model SR7, taking the rheology lines for PDMS and DC from Fig. 2 (lines b and e, respectively). The theoretical requirement of equal τ_x for PDMS and DC at their interface is demonstrated by the horizontal tie-line (L–M, Fig. 12a). The jump in $\dot{\gamma}$ at the interface of layer and matrix (L to M), the cause of strain refraction, is clearly the inverse viscosity ratio of the two materials. The 'strain intensification' within the PDMS matrix adjacent to the DC layer ($\bar{\gamma}_M = \sim 1.5$) is represented by the difference in $\dot{\gamma}$ values of B and M on the PDMS line.

Figure 12(b) illustrates that in theory, the viscosity ratio or competence contrast of two rheologically dissimilar power-law materials (here $n = 1$ and $n = 6$) should be markedly different according to the experimental strain rate.

Condition 1 is our model SR7, where the DC layer is more competent (in flow) than the PDMS host.

Condition 2, at point P where the PDMS and DC material lines cross, is where the two materials should behave in a rheologically identical fashion; i.e. homogeneously. Dixon & Tirrul (1991) chose the strain rate at the predicted crossing point for their two materials (like P in Fig. 12b) for their "estimated multilayer rolling conditions" for this same reason; the materials can be assumed to deform homogeneously.

Condition 3, shown by broken DC and PDMS lines in Fig. 12(b), would be expected at faster strain rates than at P. Now the DC layer has a lower effective viscosity than PDMS, a reversal of the viscosity (or competence) contrast given for Condition 1. This change in relative competence is a direct result of the difference in rheology between a linear material (PDMS) and a strongly strain-rate softening material, such as DC.

For the general case of deformation in rocks, where principal straining is oblique to contrasting layers, the viscosity ratio between Newtonian and non-Newtonian layers or between two non-Newtonian materials is not a constant, either in space or time. The effective viscosity contrast might be expected to change during a deformation, and so the effective viscosity contrast between the same two lithologies in different structural regimes should be very different. Ramsay (1982; also Ramsay & Huber 1987, figs. 19.20–23) present vivid examples of two rock types (e.g. limestone and marl) showing opposite senses of competence in two different regions; he explained this in terms of compositional and mineralogical changes associated with metamorphism. Our results present an alternative explanation for competence reversal, which requires no change in material composition, but arises in two rheologically dissimilar materials (e.g. Fig. 12b) solely from different deformation conditions.

Variations of strain within the simple-shear models: curving γ trajectories

These smooth strain variations will be discussed only for the simple-shear experiments where one set of grid lines represent the γ trajectories. Curving grids are also a feature of the pure-shear experiments, but the nature of this strain variation is more complex, as already noted.

The refraction theory of Treagus (1983, 1988) assumed a simple pattern of sharp strain refraction

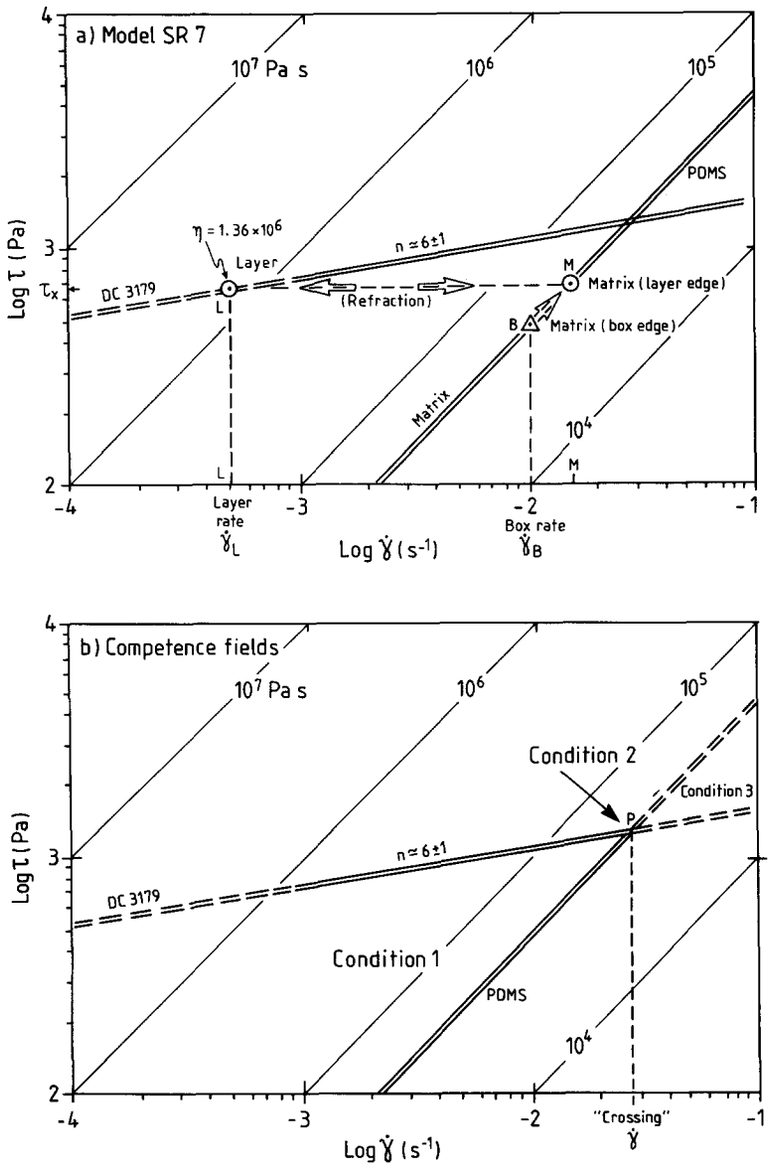

Fig. 12. (a) Rheology map illustrating the strain rate refraction for model SR7. The PDMS and DC lines are taken from Fig. 2 (lines b and e). Note the jump (L–M) in $\dot{\gamma}$ from layer to matrix. (b) The rheology map for DC and PDMS, as (a), showing the three possible competence contrast fields. See text for full discussion of both parts.

across boundaries, and uniform strain within uniform straight layers (Fig. 1). In other words, there was a constant layer-parallel shear stress component (τ_x) across the idealized multilayer system, and necessary jumps in shear strain rate across boundaries (Cobbold 1983, Cobbold *et al.* 1984). This is represented by the constant τ_x profile in Fig. 13(a).

In comparison with this theoretical model, our single-layer experiments showed sharp boundary strain refraction, but also curving γ trajectories towards the boundary (e.g. Figs. 5 and 6a). The reason for this strain gradient in the matrix is that the outer regions of the model must deform at the bulk or box rate; yet the matrix material here is not equivalent to the 'bulk rheology'. So, in effect, the confining medium for the single layer has to change from being of 'bulk behaviour' at the outer edge, into being the incompetent layer relative to the more competent single layer (for models SR2 and SR7; vice versa for SR8) adjacent to the layer. The smooth γ trajectory indicates a smooth shear stress (τ_x) gradient in the matrix from the edge towards the layer boundary, rather than a constant τ_x, but no evidence for a 'jump' in τ_x at the layer boundary (see Fig. 12a).

In a heterogeneous simple-shear flow which can be legitimately modelled as laminar or plug flow, τ should increase or decrease linearly (Truesdell 1966, p. 82, Hobbs 1972). For Newtonian fluids, γ would likewise vary in linear fashion; however, for non-Newtonian fluids, a linear increase (or decrease) in τ across a zone of shear will give rise to a non-linear increase (or decrease) in $\dot{\gamma}$, and therefore a non-linearly varying γ. For a power-law stress exponent, n, the function of γ would be proportional to τ^n. In this light, we shall reinvestigate the γ variations in our models, given by the γ and $\bar{\gamma}$ profiles described earlier.

Figure 10 showed the γ variation in normalized ($\bar{\gamma}$) form, for the PDMS matrix (Newtonian) of model SR7.

Although there is a gross linear change in γ from the edge of the box to the interface with the DC layer, there is a consistent sinuous variation about linear for all stages of the model. This may be explained in terms of the local variations from perfect simple shear caused by the accommodation of the refracted strain pattern.

The γ variations across the box for the 'half and half' model (Fig. 11) are non-linear for both the RG half (Newtonian) and the DC half, although very close to linear in RG. In theory, if both materials were in perfect simple shear with a linear change in τ_x across the box (Fig. 13b), there should be a linear $\bar{\gamma}$ trend for RG and an approximately 6th power function for DC, as described above. It is not clear from a simple inspection of $\bar{\gamma}$ for DC in Fig. 11(b) how close this curve is to exponential. We have therefore taken the $\bar{\gamma}$ data from Fig. 11(b) and used it to determine factors of the bulk strain *rate*, in order to determine the stress profile (τ_x) across the box (Fig. 14). Figure 14(a) represents the 'half and half' experiment on a simplified rheology map, comparable to Fig. 12(a) for SR7, and shows the interface τ_x tie-line joining the two different interface strain rates. Figure 14(b) shows that the τ_x profile is close to linear in a broad region either side of the viscosity boundary, but departs from linearity towards the box edges, in a symmetrical fashion. However, these are only indirect measurements of stress, which are dependent on measurement errors, so should be used reservedly as a general model.

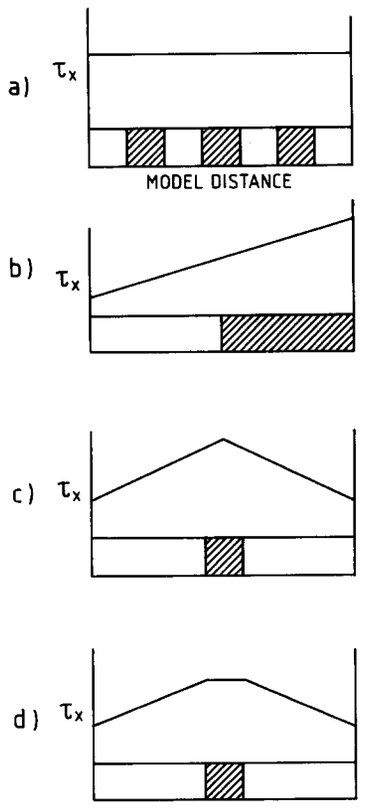

Fig. 13. Idealized τ_x profiles (x parallel to interface) across modelled systems. (a) Constant τ_x across binary multilayer, according to earlier refraction theory. (b) Linear τ_x for 'half and half' model. (c) & (d) Two alternatives for single-layer simple-shear experiments, the second a simplification of the first. Shaded layers are the more competent, in each.

Predictions of viscosity ratio assuming linear τ_x and linearly changing γ

The shear stress and strain profiles described for the models lead to the conclusion that viscosity boundaries generate gradients in τ_x within the bulk simple-shear zone. As these gradients occur both for experiments where the central layer is modelled as a rectangular inclusion, and for the 'half and half' models (one continuous viscosity boundary), we do not think they can be explained simply by the shape of the model or interface. Instead, the gradients would seem to be a necessary feature of a system where a prescribed bulk deformation (in this case, simple shear) is achieved by strongly different internal deformations within different components.

The simple-shear models documented above suggest a grossly linear change in τ_x, and thus for Newtonian materials, a linearly changing γ and $\bar{\gamma}$. On the basis of this, it is possible to use the normalized matrix boundary strain, $\bar{\gamma}_M$, which is a measure of the intensification or depletion at a viscosity boundary, to provide an alternative method of determining the viscosity ratio, or $\bar{\gamma}_M/\bar{\gamma}_L$. Figure 13(c) shows an ideal linear τ_x trend across a single-layer simple-shear model, and Fig. 15(a) shows the schematic $\bar{\gamma}$ profile for this case. In order that the total shear displacement equals the bulk (i.e. bulk $\bar{\gamma} = 1$), the two shaded areas in Fig. 15(a) must be equal. The slope of the $\bar{\gamma}$ profile for the layer is not immediately obvious, but is equal to the slope for the matrix divided by the viscosity ratio. We can approximate Fig. 15(a) to the simpler form in Fig. 15(b), where $\bar{\gamma}_L$ is taken as constant: the τ_x profile is shown in Fig. 13(d). The two shaded areas which must now be equal are

$$h_M(\bar{\gamma}_M - 1)/2 = h_L(1 - \bar{\gamma}_L), \quad (7)$$

where h_M, h_L are the half-distances of matrix and layer, respectively (Fig. 15b). This gives rise to a predicted K of

$$K = \bar{\gamma}_M/\bar{\gamma}_L = 2\bar{\gamma}_M/(2 + \alpha - \alpha\bar{\gamma}_M), \quad (8)$$

where $\alpha = h_M/h_L$. This approximation, which assumes a constant $\bar{\gamma}$ in the layer, gives predicted K values approaching the exact expression derived from Fig. 15(a), for small α and large K. It is a slight underestimate of K for $K > 1$, and overestimate for $K < 1$. The more exact expression from Fig. 15(a) is

$$K = [\bar{\gamma}_M(2\alpha + 1) - 1]/[\alpha(2 + \alpha - \alpha\bar{\gamma}_M)]. \quad (9)$$

Table 2 shows the predicted K ratios for the single-layer simple-shear models, using the exact and approximate expressions above and the model values of α and $\bar{\gamma}_M$ (average). Comparisons between these K estimates and the measured K for the models, and also the viscosity ratio from viscometry, suggest that they may provide a useful rough measure of viscosity ratio. This method would seem to be valid where K cannot be measured across a boundary; for example, where there is a measurable strain gradient towards a thin layer which has no detectable shear strain.

Finally, we must ask whether these results, based on

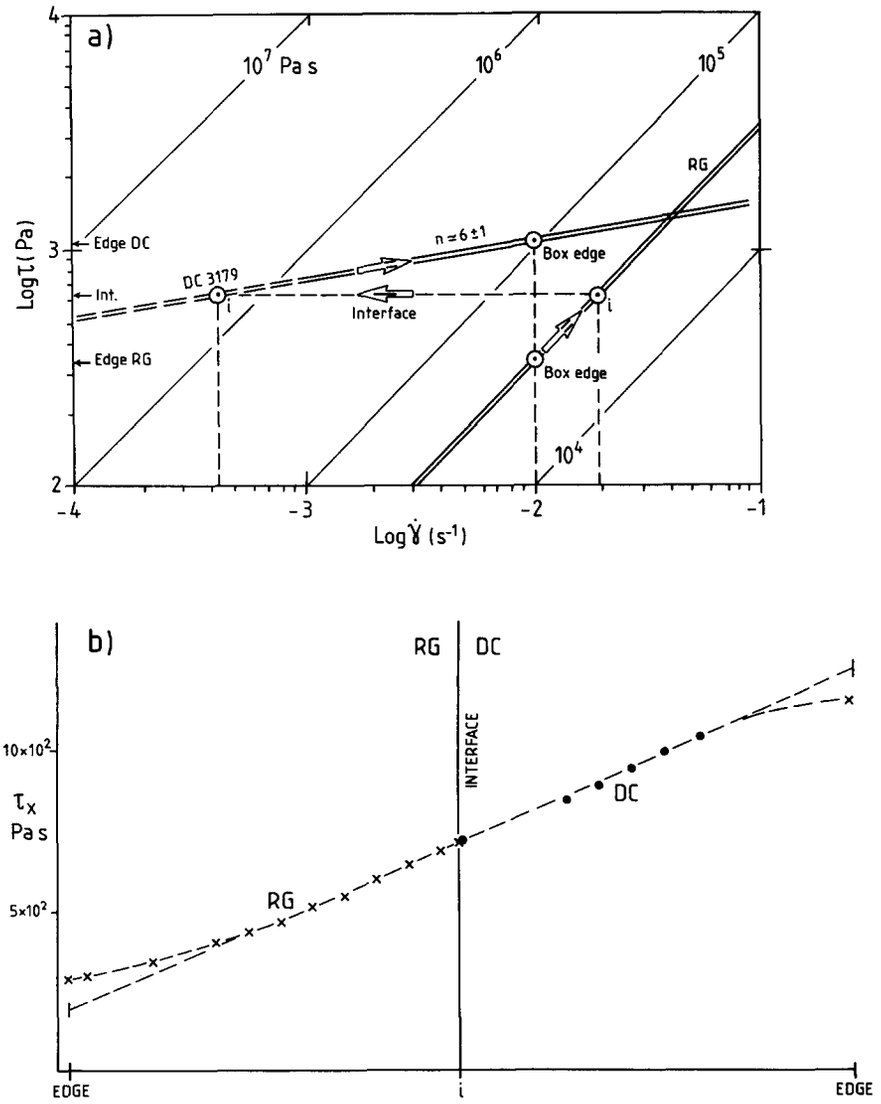

Fig. 14. (a) Rheology map for the 'half and half' model, taking the RG and DC data (lines a and e) from Fig. 2, and illustrating the jump in $\dot{\gamma}$ from RG to DC along the τ_x tie-line for the interface (labelled i). (b) τ_x profile across the model, computed by using the $\bar{\gamma}$ profiles in Fig. 11(b) to determine values of $\dot{\gamma}$, and then derive τ_x for RG and DC, from (a).

the assumption of a linear variation in τ_x, are applicable to geological strain variations. Can a linear τ_x gradient, appropriate for ideal laminar flow (Truesdell 1966, p. 81), and which Hobbs (1972) applied to heterogeneous simple shear, be used as a working approximation for more general geological deformations? We post two justifications. Firstly, it is pragmatic to begin with the simplest theoretical model, in the absence of contradictory evidence. So if geological evidence, such as curving strain trajectories, suggests stress and strain gradients, it is sensible to start by considering the simplest type of gradients (i.e. linear). Secondly, deformation in contrasting layered systems may be considered in terms of two components (Treagus 1988): a homogeneous layer-parallel pure shearing and a heterogeneous (refracting) layer-parallel simple shearing. If the latter now includes a linear gradient in this shear stress component, the compound (additive) effect will be a linear τ_x gradient. (In this general case, τ_x would not be the maximum shear stress, as it is for simple shearing alone.)

This leads us tentatively to suggest that strain gradients generated by viscosity boundaries, in more general flows than simple shear, may be characterized by linear increases or decreases of boundary-parallel shear stress. For Newtonian rheology, this implies linear changes in γ, and allows predictions of viscosity contrast to be made from shear strain increases or decreases, using the expressions above. Further investigations (by others) should reveal whether this pragmatic approach is justified, or not.

CONCLUSIONS

(1) Models using Newtonian materials confirm that the finite shear strain ratio, K, is a reliable measure of the inverse viscosity ratio. However, these experiments are for the rather special case of layer-parallel steady simple shear (i.e. only the refracting component, b, of Treagus 1988). Comparison of shear strain ratios with viscosity in pure shear experiments was found to be impractical.

(2) Power-law material in layer-parallel simple shearing at constant rate will have a constant viscosity, so will be pseudo-Newtonian. Therefore, the simple-shear models using power-law material follow the same rule as for Newtonian materials: i.e. K is a constant, and a measure of the inverse viscosity ratio. This will not be so for other deformations.

(3) The degree of strain intensification adjacent to an isolated single layer of contrasting property, seen by curving strain trajectories, may provide a rough measure of viscosity contrast, if it can be assumed that there is a linear gradient of τ_x, and Newtonian rheology.

(4) If rocks behave as non-Newtonian fluids under flow conditions, the concept of a ductility scale, and the idea of 'competence' contrast as a material property, must be rejected. The viscosity ratio which gives rise to a shear strain rate ratio, will vary in time and space, for power-law type materials. Adjacent layers with strongly different n values must be expected to behave, relatively, in a very particular fashion, determined by the bulk strain rate and the deformation history. The finite shear strain rate will be a measure of the 'net viscosity ratio', and should not be considered as a material constant.

(5) If geological data indicate that there is a constant finite shear strain ratio (K) across a lithological boundary, either regionally or around a geological structure (meso- or macro-scale), and the deformation is clearly not simple shear, this is evidence of a constant viscosity ratio (or competence ratio), in time and space. We suggest this is a good indication that both lithologies flowed under approximately Newtonian conditions.

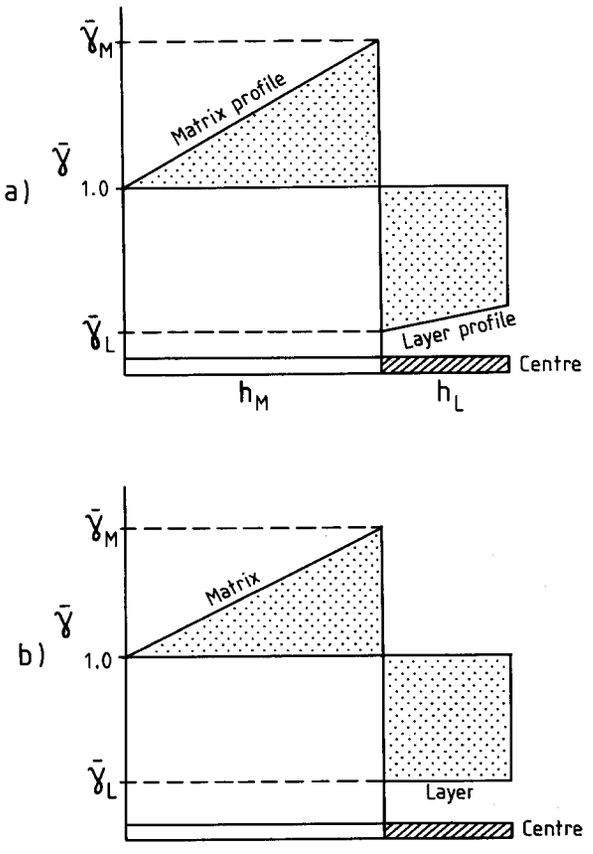

Fig. 15. Schematic profiles of $\bar{\gamma}$ across a single-layer simple-shear model, based on a linear τ_x profile and Newtonian rheology. (a) Using the τ_x profile in Fig. 13(c), and (b) using the simplified profile in Fig. 13(d). To maintain bulk displacement, the two shaded areas must be equal in both cases.

Acknowledgements—This work is the outcome of a European Science Exchange program funded by the Royal Society of Britain and the Royal Swedish Academy of Science for S. H. Treagus to work in the Hans Ramberg Laboratory at Uppsala. S. H. Treagus would like to thank Chris Talbot for welcoming this exchange, and to thank him and Rosemary Talbot for their kindness and hospitality during this visit. She also acknowledges an Honorary Research Fellowship at the University of Manchester which enabled this paper to be written. D. Sokoutis would like to thank Roberto Weinberg for his help with viscosity measurements. We are both grateful to Chris Talbot, Genene Mulugeta, Sandy Cruden and Harro Schmeling at the Geological Institute at Uppsala, for advice and comments at various stages of this work, and to the review comments from Peter Cobbold, Mel Stauffer and Peter Hudleston. Mrs Ch. Wernström is thanked for drafting the figures.

REFERENCES

Arnbom, J.-O. 1976. Experimental buckling of competent viscous sheets in a less competent viscous matrix. *Geol. För. Stockh. Förh.* **98**, 348–354.

Carter, N. L. & Tsenn, M. C. 1987. Flow properties of continental lithosphere. *Tectonophysics* **136**, 27–63.

Cobbold, P. R. 1983. Kinematic and mechanical continuity at a coherent interface. *J. Struct. Geol.* **5**, 341–349.

Cobbold, P. R., Means, W. D. & Bayly, M. B. 1984. Jumps in deformation gradients and particle velocities across propagating coherent boundaries. *Tectonophysics* **108**, 283–298.

Dixon, J. M. & Summers, J. M. 1985. Recent developments in centrifuge modelling of tectonic processes: equipment, model construction techniques and rheology of model materials. *J. Struct. Geol.* **7**, 83–102.

Dixon, J. M. & Summers, J. M. 1986. Another word on the rheology of silicone putty: Bingham. *J. Struct. Geol.* **8**, 593–595.

Dixon, J. M. & Tirrul, R. 1991. Centrifuge modelling of fold-thrust structures in a tripartite stratigraphic succession. *J. Struct. Geol.* **13**, 3–20.

Fletcher, R. C. 1974. Wavelength selection in the folding of a single layer with power-law rheology. *Am. J. Sci.* **274**, 1029–1043.

Handy, M. R. 1990. The solid-state flow of polymineralic rocks. *J. geophys. Res.* **95**, 8647–8661.

Hobbs, B. E. 1972. Deformation of non-Newtonian materials in simple shear. In: *Flow and Fracture of Rocks* (edited by Heard, H. C., Borg, I. Y., Carter, N. L. & Raleigh, C. B.). *Am. Geophys. Un. Geophys. Monogr.* **16**, 243–258.

Hudleston, P. J. & Holst, T. B. 1984. Strain analysis and fold shape in a limestone layer and implications for layer rheology. *Tectonophysics* **106**, 321–347.

Kirby, S. H. & Kronenberg, A. K. 1987. Rheology of the lithosphere: selected topics. *Rev. Geophys.* **25**, 1219–1244.

Lister, G. S. & Williams, P. F. 1983. The partitioning of deformation in flowing rock masses. *Tectonophysics* **92**, 1–33.

Mancktelow, N. S. 1988. The rheology of paraffin wax and its usefulness as an analogue for rocks. *Bull. geol. Instn. Univ. Uppsala* **14**, 181–193.

McClay, K. R. 1976. The rheology of plasticine. *Tectonophysics* **33**, T7–T15.

Means, W. D. 1990. Review paper—Kinematics, stress, deformation and material behavior. *J. Struct. Geol.* **12**, 953–972.

Onogi, S. & Matsumoto, T. 1981. Rheological properties of polymer solutions and melts containing suspended particles. *Polym. Engng Rev.* **1**, 45–87.

Paterson, M. S. 1987. Problems in the extrapolation of laboratory rheological data. *Tectonophysics* **133**, 33–43.

Ramsay, J. G. 1980. Shear zone geometry: a review. *J. Struct. Geol.* **2**, 83–100.

Ramsay, J. G. 1982. Rock ductility and its influence on the develop-

ment of tectonic structures in mountain belts. In: *Mountain Building Processes* (edited by Hsü, K. J.). Academic Press, London, 111–127.

Ramsay, J. G. & Huber, M. I. 1987. *The Techniques of Modern Structural Geology, Volume 2: Folds and Fractures*. Academic Press, London.

Schmid, S. M. 1982. Microfabric studies as indicators of deformation mechanisms and flow laws operative in mountain building. In: *Mountain Building Processes* (edited by Hsü, K. J.). Academic Press, London, 95–110.

Sokoutis, D. 1967. Finite strain effects in experimental mullions. *J. Struct. Geol.* **9**, 233–242.

Talbot, C. J. 1983. Microdiorite sheet intrusions as incompetent time- and strain-markers in the Moine assemblage NW of the Great Glen fault, Scotland. *Trans. R. Soc. Edinb.* **74**, 137–152.

Treagus, S. H. 1972. Processes in fold development. Unpublished Ph.D. thesis, University of Manchester.

Treagus, S. H. 1973. Buckling stability of a viscous single-layer system oblique to the principal compression. *Tectonophysics* **19**, 271–289.

Treagus, S. H. 1981a. A theory of stress and strain variations in viscous layers, and its geological implications. *Tectonophysics* **72**, 75–103.

Treagus, S. H. 1981b. A simple-shear construction from Thomson & Tait (1867). *J. Struct. Geol.* **3**, 291–293.

Treagus, S. H. 1983. A theory of finite strain variation through contrasting layers, and its bearing on cleavage refraction. *J. Struct. Geol.* **5**, 351–368.

Treagus, S. H. 1988. Strain refraction in layered systems. *J. Struct. Geol.* **10**, 517–527.

Truesdell, C. 1966. *Elements of Continuum Mechanics*. Springer, New York.

Truesdell, C. & Noll, W. 1965. Non-linear field theories of mechanics. In: *Handbuch der Physik*, Vol. 3 (edited by Flügge, S.). Springer, Berlin.

Tsenn, M. C. & Carter, N. L. 1987. Upper limits of power law creep of rocks. *Tectonophysics* **136**, 1–26.

Weijermars, R. 1986a. Flow behaviour and physical chemistry of bouncing putties and related polymers in view of tectonic laboratory applications. *Tectonophysics* **124**, 325–358.

Weijermars, R. 1986b. Polydimethylsiloxane flow defined for experiments in fluid dynamics. *Appl. Phys. Lett.* **48**, 109–111.

Weijermars, R. 1986c. Finite strain of laminar flows can be visualized in SGM36-polymer. *Naturwissenschaften* **73**, S33.

Weijermars, R. & Schmeling, H. 1986. Scaling of Newtonian and non-Newtonian fluid dynamics without inertia for quantitative modelling of rock flow due to gravity (including the concept of rheological similarity). *Phys. Earth & Planet. Interiors* **43**, 316–330.